SLC45A4 encodes a mitochondrial putrescine transporter that promotes GABA *de novo* synthesis

Cecilia Colson,[1#] Yujue Wang,[1,2#$] James Atherton,[1] and Xiaoyang Su[1,2,*]

[1]Department of Medicine, Rutgers-Robert Wood Johnson Medical School, New Brunswick, NJ 08901, USA. [2]Rutgers Cancer Institute of New Jersey, New Brunswick, NJ 08903, USA. # These authors contributed equally to this work $ Current address: School of Pharmaceutical Sciences, Tsinghua-Peking Center for Life Sciences, Beijing Frontier Research Center for Biological Structure, Tsinghua University, Beijing, China *e-mail: xs137@rwjms.rutgers.edu (X.S.)

ABSTRACT

Solute carriers (SLC) are membrane proteins that facilitate the transportation of ions and metabolites across either the plasma membrane or the membrane of intracellular organelles. With more than 450 human genes annotated as SLCs, many of them are still orphan transporters without known biochemical functions. We developed a metabolomic-transcriptomic association analysis, and we found that the expression of SLC45A4 has a strong positive correlation with the cellular level of γ-aminobutyric acid (GABA). Using mass spectrometry and the stable isotope tracing approach, we demonstrated that SLC45A4 promotes GABA *de novo* synthesis through the Arginine/Ornithine/Putrescine (AOP) pathway. SLC45A4 functions as a putrescine transporter localized to the mitochondrial membrane to facilitate GABA production. Taken together, our results revealed a new biochemical mechanism where SLC45A4 controls GABA production.

INTRODUCTION

Individual cells use channels and transporters embedded in the lipid membranes to exchange chemicals such as water, ions, nutrients, vitamins, cofactors, and many drugs with their environments.[1,2] Solute carrier (SLC) transporter family, comprised of 458 members distributed in 65 subfamilies,[3] is the second-largest family of membrane proteins in the human genome next to G-protein-coupled receptors (GPCRs).[4–8] Not only SLC transporters are fundamental to cellular metabolism, but they also show clear links to human diseases. Based on Open PHACTS, a platform that integrates disease, chemical, and target databases, at least 190 different SLCs have been found mutated in human disease.[9–11] Despite increasing interest and the emergence of database ontology, around 30% of SLCs are still uncharacterized and remain orphan transporters with unidentified substrates, particularly when it concerns transporters with endogenous compounds.[12] In this work, we developed a metabolomic-transcriptomic association analysis, and we discovered that the expression of *SLC45A4* has a strong positive correlation with the cellular level of γ-aminobutyric acid (GABA).

The function of SLC45A4 is largely unknown. It has been annotated as a proton(H^+)-associated sucrose transporter based on its homology to the sucrose transporter (SUC) genes in *Arabidopsis thaliana*.[13] In *Saccharomyces cerevisiae*, mouse *Slc45a4* restores the growth of a strain incapable of sucrose uptake. However, in a recent study, Meixner, E., et al manually established a substrate-base ontology to identify potential substrates for orphan SLCs.[14] Their results suggest that SLC45A4 and its homolog SLC45A3 could be transporter for metal ions but they did not identify carbohydrates as potential substrates. In mammalian cells, SLC45A4 was implicated in different types of cancers and associated with different clinical outcomes regarding the type of cancer. For example, SLC45A4 gene expression is positively associated with tumor suppression in osteosarcoma[15] but higher risk in cancer pancreatic ductal adenocarcinoma.[16] SLC45A4 is mostly described as a biomarker of clinical severity of cancer but its mechanisms are poorly understood.

GABA was first discovered in mammalian brains over half a century ago.[17,18] Besides its presence in the central nervous system, GABA has also been identified in many organs including the pancreas, pituitary, testes, gastrointestinal tract, ovaries, placenta, uterus, and adrenal medulla.[19] The metabolic and signaling role of GABA in peripheral tissue is relatively poorly understood. GABA signalling has been associated with stem cell proliferation,[20] implicating its importance in cancer progression. Lastly, a study revealed that GABA treatment of mice developing triple-negative breast cancer was promoting metastasis to the lung and brain.[21] There are two GABA synthesis pathways in mammals: In GABAergic neurons, GABA is synthesized by glutamic acid decarboxylase (GAD) enzymes.[22] In addition to this canonical GAD pathway, GABA can also be produced via the arginine-ornithine-putrescine (AOP) pathway.[23,24] Putrescine can be oxidized in tandem reactions catalyzed by diamine oxidases (DAOs)[25,26] or monoamine oxidases (MAOs)[27,28], and aldehyde dehydrogenases (ALDHs)[29,30] to produce GABA. Interestingly, dopaminergic neurons in the midbrain rely on the AOP pathway for GABA synthesis,[31] demonstrating the importance of this pathway in GAD-negative cells and tissues. Our findings, that SLC45A4 promotes GABA *de novo* synthesis via the AOP pathway, reveal a new layer of the regulation of GABA metabolism in mammalian cells.

RESULTS

Transcriptomic-Metabolomic association analysis reveals the role of SLC45A4 in GABA metabolism

Our overarching goal is to systematically investigate the biochemical functions of orphan SLC transporters. Our approach is to link the gene expression levels and the metabolite levels through a transcriptomic-metabolomic association analysis. We leveraged publicly available datasets from the Cancer Cell Line Encyclopaedia (CCLE),[32,33] and we built linear regression models to analyze the expression levels of 56,202 human genes and the cellular levels of 225 metabolites in 928 human cancer cell lines. For each model, we calculated the t-value for the slope. As expected, a number of SLC genes showed strong correlations with cellular metabolite levels (Supp Figure 1). For example, we found a strong positive correlation between cellular creatine levels and the expression levels of *SLC6A8* (Supp Figure 2), which is a known creatine transporter.[34] In fact, *SLC6A8* shows the highest positive correlation with cellular creatine levels out of >56,000 transcripts in the CCLE dataset (Figure 1a). Similarly, cellular carnitine levels are strongly correlated with the expression levels of *SLC22A5* (Figure. 1a), a known carnitine transporter;[35] and cellular taurine levels are strongly correlated with the expression levels of *SLC6A6* (Figure. 1a), a known taurine transporter.[36] These results demonstrate that the transcriptomic-metabolomic association analysis is capable of revealing genes responsible for cellular metabolite accumulation. Interestingly, we found that cellular GABA levels are strongly correlated with the expression levels of *SLC45A4* (Figure. 1a). SLC45A4 shows a much stronger positive correlation with cellular GABA levels than the known GABA transporters (GAT1:SLC6A1, GAT2:SLC6A13, and GAT3:SLC6A11) and the GABA producing enzymes (GAD1, GAD2) (Supp Figure 3). The current annotation of SLC45A4 as a proton(H^+)-associated sucrose transporter[13] is insufficient in explaining its role in GABA metabolism, so we set out to investigate the biochemical function of this gene.

To experimentally verify the transcriptomic-metabolomic associations identified from CCLE, we chose three human cell lines to work on: A549 and H1299 cells that express relatively high levels of *SLC45A4*, and HepG2 cells that express very low levels of *SLC45A4* as confirmed by relative mRNA quantification (Figure. 1b). We also measured the cellular GABA level using LC-MS. As predicted, we detected a lower level of GABA in HepG2 cells compared to the other two cell lines (Figure 1b). To demonstrate that the expression level of *SLC45A4* has a direct causal relationship with the cellular GABA level, we transiently overexpressed (OE) SLC45A4 in HepG2 cells. The LC-MS results showed a higher level of GABA in the *SLC45A4* OE cells (Figure. 1c.), demonstrating that *SLC45A4* controls cellular GABA levels.

2

SLC45A4 increases cellular GABA levels by facilitating GABA *de novo* synthesis

Next, we inquired: how does SLC45A4 affect cellular GABA levels? First, we tested the hypothesis that SLC45A4 works as a sucrose transporter. A549 and H1299 cells were cultured in $^{13}C_6$-glucose with or without supplemented ^{12}C-sucrose. If sucrose is catabolized by these cells, it should be incorporated into the glycolytic and the TCA cycle intermediates, and therefore decrease the ^{13}C enrichment in these metabolites. Our observations denied this hypothesis. While we observed a robust ^{13}C labeling in glycolysis and TCA cycle intermediates, the addition of sucrose has no negative impact on them, suggesting sucrose is not catabolized (Supp Figure 4). Meanwhile, we observed very little ^{13}C labeling (<1%) in GABA when $^{13}C_6$-glucose was used as the tracer. Therefore, the impact on GABA synthesis cannot be explained by the putative sugar transporter activity of SLC45A4.

The next obvious hypothesis is that SLC45A4 functions as a GABA transporter facilitating GABA uptake. To evaluate this potential GABA transporter activity, we fed stable isotope-labeled GABA ($^{13}C_4$-GABA) to control and *SLC45A4* Knock Down (KD) A549 and H1299 cells (Figures. 1d and 1e.). In both cell lines, we observed decreases in total GABA levels when SLC45A4 was knocked down, confirming the role of SLC45A4 in GABA metabolism. However, we found that the decrease in GABA level was mainly due to a decline in endogenous, unlabeled GABA ($^{12}C_4$-GABA) rather than a decline in the uptake of $^{13}C_4$-GABA (Figure. 1e). Our untargeted metabolomics analysis picked up 2,676 features from this dataset (Figure. 1f). The top 4 hits that are most significantly changed in the KD cells are all related to unlabeled GABA (the protonated ion $[M+H]^+$, the protonated ion with a water loss $[M+H-H_2O]^+$, ^{13}C isotope natural abundance ion $[^{13}C_1-M+H]^+$, and ^{13}C isotope natural abundance ion with a water loss $[^{13}C_1-M+H-H_2O]^+$). The $^{13}C_4$-GABA, which indicates GABA uptake, was only slightly changed in A549 KD cells but not in H1299 KD cells. These results indicate that although it regulates cellular GABA levels, SLC45A4 does not function directly as a GABA transporter. From these results, we inferred that SLC45A4 is required for the *de novo* synthesis of GABA.

Ornithine is the major source of GABA *de novo* synthesis in human cancer cells

To investigate the role of SLC45A4 in GABA *de novo* synthesis, we explored different GABA biosynthetic routes in A549 and H1299 cells. The most well-studied GABA synthesis route is through glutamate decarboxylation (GAD pathway) in GABAergic neurons (Figure. 2a), while other tissues have been reported for using arginine, ornithine, or putrescine as sources for GABA (AOP pathway).[37] Therefore, we fed the cells with either $^{13}C_5$-glutamine or $^{13}C_6$-arginine as the tracer, and we measured the ^{13}C incorporation in GABA (Figures. 2b and 2c). $^{13}C_5$-glutamine produced a significant amount of $^{13}C_5$-glutamate, but it labeled <6% of GABA (Figure. 2b). On the other hand, $^{13}C_6$-arginine labeled >30% GABA with ^{13}C (Figure. 2c), suggesting that the AOP pathway is the dominant pathway for GABA synthesis in A549 and H1299 cells. In fact, our transcriptomic-metabolomics association study not only identified *SLC45A4* as the top gene related to GABA production, but it also revealed that ornithine decarboxylase (*ODC1*), which converts ornithine to putrescine, is the gene with the second-highest positive correlation with cellular GABA levels out of >56,000 transcripts assessed (Supp Figure 1). These results support the idea that SLC45A4 promotes GABA synthesis through the AOP pathway.

Interestingly, when culturing cells in $^{13}C_6$-arginine, we observed a robust extracellular production of $^{13}C_5$-ornithine (Figure. 2c), which raised the question of whether ornithine is an important substrate for GABA *de novo* synthesis in the presence of arginine. Although ornithine is not proteogenic and is often omitted from most cell culture media, it was found to be present at roughly 200 µM in plasma and 300 µM in the tumor interstitial fluid.[38] In cell culture, the extracellular production of ornithine happened because the fetal bovine serum (FBS) we used contains arginase activity, which breaks down the arginine in the RPMI 1640 media to ornithine (Figure. 2d). To avoid the extracellular ornithine production, we heat-inactivated the FBS at 70°C, which is effective in eliminating arginase activity (Figure. 2e). Using the heat-inactivated FBS (hiFBS), we prepared RPMI media containing $^{13}C_6$-

arginine (1.15 mM) and $^2H_6$-ornithine (200 µM). Surprisingly, our results showed that in A549 and H1299 cells, 98% of labeled GABA were ^2H-labeled (both $^2H_6$- and $^2H_4$-GABA were generated due to the molecular symmetry of putrescine) (Figure. 2f and Supp Figure 5) which suggested that they were derived from ornithine. Less than 2% of labeled GABA were ^{13}C-labeled indicating that only a small fraction of GABA was derived from arginine. These observations indicated that ornithine is the preferred substrate for GABA biosynthesis.

SLC45A4 promotes GABA *de novo* synthesis from ornithine and putrescine

Knowing that GABA *de novo* synthesis mostly comes from ornithine, we first tested whether the overexpression of SLC45A4 would enhance GABA production from ornithine. Indeed, when *SLC45A4* is overexpressed in HepG2 cells, a greater amount of $^2H_6$-GABA made from $^2H_6$-ornithine was detected (Figure. 2g). The next question is whether SLC45A4 is strictly required for GABA synthesis from ornithine. To answer this question, we generated *SLC45A4* KO cell lines in both A549 and H1299 backgrounds (Figures. 3a and 3b). Then, we cultured the WT and KO cells with $^2H_6$-ornithine, and we observed that the *SLC45A4* KO significantly decreased the production of GABA from ornithine, but did not completely eliminate it (Figure. 3c.). Interestingly, we also observed the accumulation of $^2H_6$-putrescine in the KO cells (Figure. 3d.), suggesting putrescine oxidation might be impeded in *SLC45A4* KO cells.

To explore the role of SLC45A4 in ornithine and putrescine metabolism, we performed a $^2H_6$-ornithine and $^{13}C_4$-putrescine dual-tracing experiment (Figure. 3e). Putrescine, the decarboxylation product of ornithine, is the downstream intermediate for GABA biosynthesis. Interestingly, we observed a differential effect of *SLC45A4* KO on ornithine and putrescine metabolism in GABA production. As shown in Figure. 3f, *SLC45A4* KO significantly decreased the level of $^2H_6$-GABA. However, *SLC45A4* KO did not affect the level of $^{13}C_4$-GABA (Figure. 3g.), which suggests that SLC45A4 may not be required for extracellular putrescine oxidation to produce GABA. These results create a conundrum. On one hand, *SLC45A4* KO results in an intracellular build-up of putrescine and decreased GABA production, pointing to a bottleneck in putrescine oxidation. On the other hand, *SLC45A4* KO cells show no deficiency in converting supplemented putrescine to GABA. To resolve this conundrum, we explored another approach to increasing intracellular putrescine levels by overexpressing *ODC1*. As mentioned before, *ODC1* has the second-highest correlation with GABA levels revealed by our transcriptomic-metabolomic analysis. In fact, inhibition of ODC1 by DFMO (Figure. 4a) decreases cellular putrescine and GABA levels in both H1299 cells and in HepG2 cells overexpressing *SLC45A4* (Figures. 4b. and 4c.). In parallel, ODC1 overexpression increases both cellular putrescine and GABA levels (Figure. 4d.). However, the ODC1 overexpression did not fully rescue the deficiency in GABA production in SLC45A4 KO cells, suggesting SLC45A4 is required for efficient putrescine oxidation. The seemingly conflicting results from putrescine supplementation and *ODC1* overexpression hinted to us to consider how the intracellular and extracellular putrescine is oxidized.

Depending on the cell types, GABA can be produced either through DAO or MAO. To test which pathway is active in A549 and H1299 cells, we treated the cells with various DAO and MAO inhibitors (Figure. 4a). Pentamidine and aminoguanidine are inhibitors of diamine oxidases,[39,40] which are Cu(II)-dependent enzymes. Clorgyline is a specific inhibitor of MAO-A,[41] and selegiline is a specific inhibitor of MAO-B,[42] both are flavin adenine dinucleotide (FAD)-dependent enzymes.[43] All the DAO inhibitors showed inhibition of GABA production from $^2H_6$-ornithine, but neither of the MAO inhibitors did (Figure. 4e). In addition, LCC-12, a mitochondrial Cu(II) chelator,[44] also inhibited GABA production from ornithine without any effect on putrescine levels (Figure. 4f). All these results suggest GABA is produced from putrescine through DAO activities. One potential confounding factor is the diamine oxidase activity in FBS. Although the purified serum DAO shows

4

poor activity on putrescine,[45,46] we suspect that this enzymatic activity contributes to the oxidation of extracellular putrescine nonetheless. To study the cellular GABA production pathway without the interference of extracellular diamine oxidase activity, we supplemented the cells with $^2H_6$-ornithine and $^{13}C_4$-putrescine treated or not with aminoguanidine. As expected, aminoguanidine decreases total cellular GABA (Fig. 4g, left) but $^2H/^{13}C$ ratio increases by 8 folds (Fig. 4g, right), indicating that GABA derived from extracellular putrescine (^{13}C fraction) is reduced (50% reduction, Supp. Fig. 6) while GABA derived from intracellular putrescine (^2H fraction) is augmented (4 folds, Supp. Fig. 6). These results suggest that supplemented putrescine is oxidized extracellularly and support hypothesis that extracellular and intracellular putrescine are enzymatically processed in different ways. We could speculate that this will explain why supplemented putrescine is converted into GABA in SLC45A4-KO cells whereas putrescine derived from ornithine is not. This suggests that SLC45A promotes GABA from ornithine and intracellular putrescine while extracellular putrescine is processed in a SLC45A4-independent manner.

SLC45A4 encodes a mitochondrial putrescine transporter

We were intrigued by the observation that GABA synthesis is inhibited by LCC-12, which specifically accumulates in mitochondria and targets mitochondrial Cu(II).[44] We wondered if GABA synthesis is compartmentalized to mitochondria. In fact, a number of SLC transporters are known to be intracellular transporters. For example, the members of the SLC25 family are mostly mitochondrial transporters,[47] and the members of the SLC35 family are mostly localized to Golgi and endoplasmic reticulum (ER).[48] SLC45A2, another member of the SLC45 family, has been found to be a melanosome transporter.[49,50] We used immunofluorescence microscopy to investigate the subcellular localization of SLC45A4. In A549 cells, we transiently overexpressed SLC45A4 with a C-terminal GFP tag. The GFP signal was clearly detected around the cell nucleus, without overlapping actin signal (Figure. 5a top panel), strongly suggesting that SLC45A4 is an organellar transporter rather than a plasma membrane transporter. In addition, the fluorescence signals of SLC45A4-GFP proteins overlapped with the signals from the MitoTracker™ dye, suggesting the mitochondrial localization of the SLC45A4 transporter (Figure. 5a middle panel). To verify these results, we made another construct of A549 cells stably overexpressing HA-tagged SLC45A4. The HA-tagged SLC45A4 also showed co-localization with MitoTracker™ dye (Figure. 5a). To further prove the mitochondrial localization of SLC45A4, we isolated mitochondria from A549 cells. The SLC45A4 protein was detected in the mitochondrial fraction along with the mitochondrial-specific marker, Citrate Synthase (CS). SLC45A4 protein was absent when specific markers for the plasma membrane and cytosol markers were detected, ATP1A1 and actin beta (ACTB) respectively (Figure. 5b). These results confirm the mitochondrial localization of SLC45A4.

Finally, we investigated what substrate is transported into mitochondria by SLC45A4 and whether GABA synthesis depends on it. The major mitochondrial ornithine transporter has been known as ORNT1 (also known as SLC25A15).[51] The mitochondrial putrescine transporter was reported to be dependent on the mitochondrial membrane potential $\Delta\psi$, but the encoding gene was never cloned.[52] Our experimental results ruled out the possibility that SLC45A4 works as an ornithine transporter. Our conclusion is based on the observation that both the WT and KO cells cultured with $^2H_6$-ornithine were able to produce $^2H_5$-proline (Figure. 5c). This biosynthetic process depends on the activities of two mitochondrial enzymes, ornithine aminotransferase (OAT) and pyrroline-5-carboxylate reductase (PYCR).[53,54] Therefore, the production of $^2H_5$-proline depends on the mitochondrial availability of ornithine. Comparing the SLC45A4 WT and KO cells, the $^2H_5$-proline production is not affected, suggesting that the supply of mitochondrial ornithine does not depend on SLC45A4. Next, to examine the activity of SLC45A4 as a putrescine transporter, we performed a ^3H-putrescine uptake assay using the mitochondria isolated from WT and *SLC45A4* KO A549 cells. WT cells showed robust putrescine uptake activity, which can

be suppressed by competition in the presence of 1 mM of unlabeled putrescine. *SLC45A4* KO, on the other hand, significantly decreased the mitochondrial putrescine uptake activity (Figure. 5d). Meanwhile, using mitochondria isolated from WT cells, we were able to detect the formation of $^{13}C_4$-GABA from $^{13}C_4$-putrescine (Figure. 5d), suggesting the putrescine oxidation activity resides in the mitochondria. Isolated mitochondria from SLC45A4 KO cells also showed lower GABA levels compared to mitochondria from WT cells (Supp Fig. 7). Taken together, our results revealed that SLC45A4 functions as a mitochondrial putrescine transporter to support GABA synthesis.

DISCUSSION

CCLE Database is an invaluable resource for the multi-omics characterization of human cancer cell lines.[32,33,55] Previous works have identified point mutations, copy number variations, and DNA methylations that may impact cellular metabolite levels.[33] In this work, we developed a transcriptomic-metabolomic association analysis, which revealed the function of SLC45A4 in GABA metabolism. Interestingly, while several transporter genes show strong correlations with the levels of cellular metabolites, the cellular level of 1-methylnicotinamide (1-MNA) is strongly correlated with nicotinamide N-methyltransferase (NNMT) expression, the synthesizing enzyme of this metabolite.[56] This discovery, together with ours, demonstrates the utility of the CCLE database in understanding fundamental biochemistry.

Our transcriptomic-metabolomic association analysis demonstrated that cellular levels of creatine, carnitine, and taurine are mostly determined by the expression of their corresponding transporters. This result suggests that in many cases, cells don't perform *de novo* synthesis of these metabolites. Instead, cultured cells take them from the media, presumably from the serum component. In light of this, it is conceivable that dialyzed FBS, compared to regular FBS, may affect cell metabolism due to its lack of key metabolic factors.

Despite the fact that SLC45A4 has a high correlation with the cellular GABA level, unlike other transporters showing high correlations with their cellular substrates, SLC45A4 is not a GABA transporter. This observation shows that the substrate selectivity and the metabolic consequence of a transporter can be very different. This is true, particularly for subcellular transporters. MFSD12, for example, mediates the import of cysteine into lysosomes and melanosomes and is required for the synthesis of the red skin pigment pheomelanin.[57] SLC22A14, a mitochondrial riboflavin transporter, is required for fatty acid oxidation and ATP production, and would eventually affect spermatozoa function and male fertility. Therefore, it is important to understand both the biochemical activities of SLC transporters and their metabolic consequences.

Literature on the SLC45A4 is scarce and mainly focuses on gene expression and associated phenotype, as we are the first to investigate its subcellular mechanism. So far, SLC45A4 expression has been linked to clinical outcomes in various cancers[15,16] but remained an orphan transporter. In this study, we discovered that SLC45A4 promotes GABA *de novo* synthesis in human cancer cells. Whether these effects depend on the GABA signaling awaits further studies.

It is conceivable that SLC45A4 may facilitate the transportation of other molecules across the mitochondrial membrane. In fact, SLC45A4 has been shown to be required for paraquat-induced cell death.[58] Reczek et al. created SLC45A4 KO cells and observed that the KO cells are resistant to paraquat-induced cell death. The whole-cell uptake of paraquat was not affected by SLC45A4 KO. It would be interesting to know whether the mitochondrial uptake of paraquat is impaired in SLC45A4 KO cells.

One limitation of our study is that we don't have a comprehensive analysis of cellular polyamines including spermidine and spermine. This is due to the fact that these compounds are too polar to be eluted well from HILIC columns. These compounds are typically chemically derivatized to be more accurately quantified on LC-MS. Given our results SLC45A4 is a mitochondrial putrescine transporter. It is possible that the polyamine synthesis pathway is also under the regulation of SLC45A4. In fact, the polyamine spermidine (downstream of putrescine)

is directly involved in proliferation by its role in the hypusination of *EIF5A* (Eukaryotic Translation Initiation Factor 5A).[59,60] Further studies on the role of SLC45A4 on polyamine metabolism are warranted.

Finally, the function of *SLC45A4* may exceed the transporter protein it encodes. Through alternative splicing, the genetic locus of *SLC45A4* produces a circular RNA named circSLC45A4. circSLC45A4, which is unlikely to encode a fully functional transporter, is highly expressed in the human fetal cortex and is required to keep neural cells in a progenitor state.[61] The physiological role of *SLC45A4* is multi-faceted.

Figure 1. SLC45A4 modulates cellular GABA levels but is not a GABA transporter.
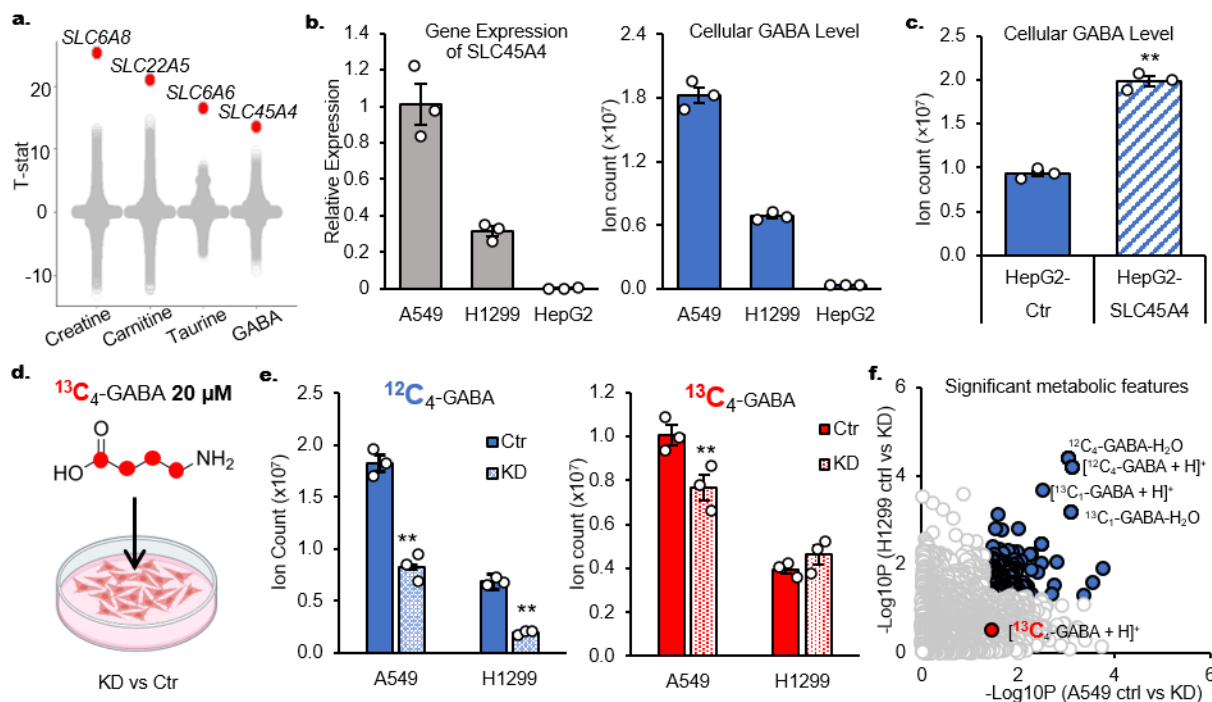

Figure 1. SLC45A4 modulates cellular GABA levels but is not a GABA transporter.

a. Association between metabolites and the expression of 54271 genes. Each point represents a gene. Genes with the strongest association are colored in red. **b.** Relative mRNA expression of *SLC45A4* (left) and cellular GABA level (right) in A549, H1299 and HepG2 cells. **c.** Cellular GABA level in HepG2 cells overexpressing empty vector (Ctr) or SLC45A4. **d.** Schematic of $^{13}C_4$-GABA supplementation in cell media. **e.** Cellular GABA level in A549 and H1299 cells transfected with scramble siRNA (Ctr) or si-SLC45A4 (KD) and cultured with 5 μM $^{13}C_4$ GABA for 24h. **f.** Metabolomes of A549 and H1299 cells transfected with scramble siRNA (Ctr) or si-SLC45A4 (KD) and cultured with 5 μM $^{13}C_4$ GABA for 24h. Each point in the scatter plot represents a metabolite. Metabolites showing significant difference between Ctr and KD in both cell lines are colored in blue. In all figures, data are mean ± SEM; n represents biologically independent replicates. **P<0.01; *P<0.05; ns, not significant by two-sided Student's t-test.

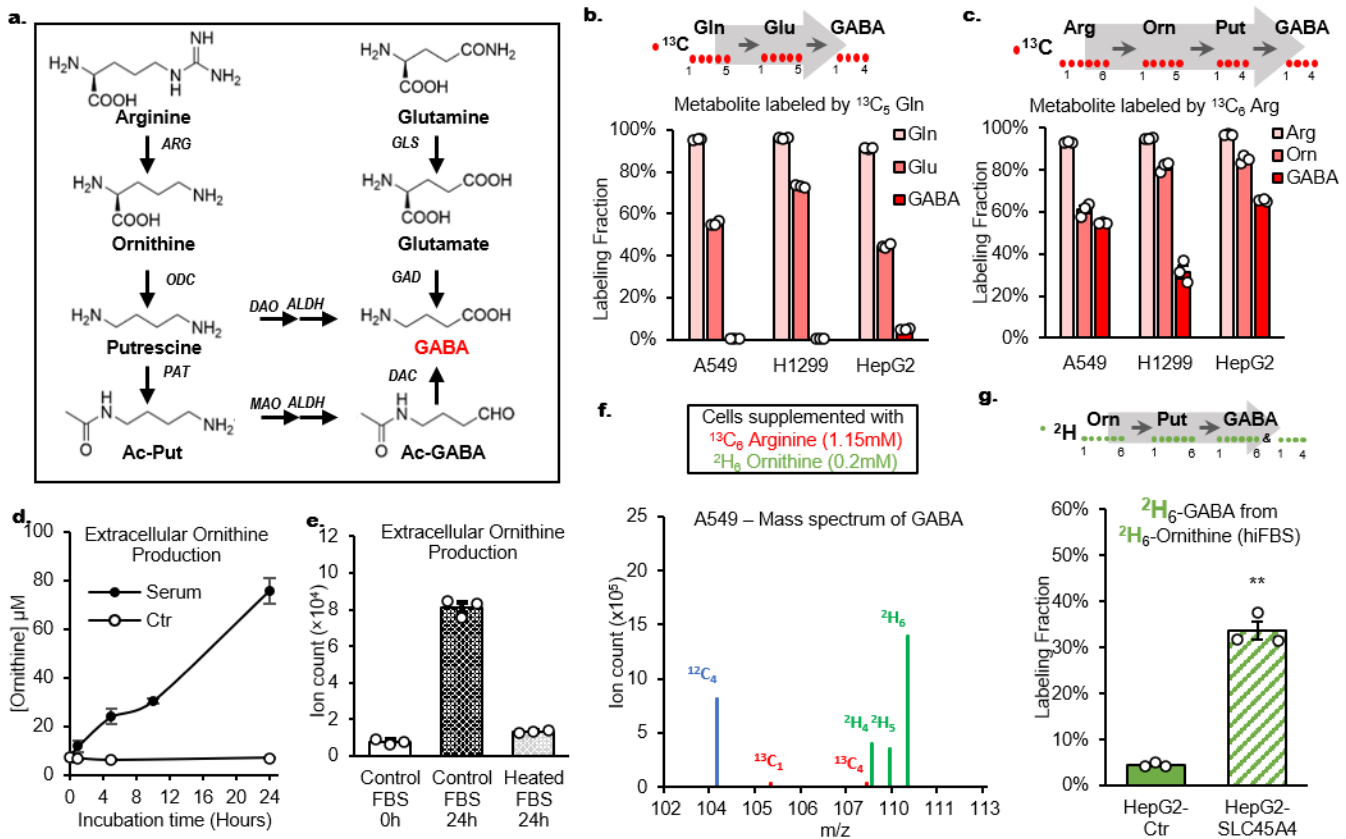Figure 2. Cellular GABA is produced from extracellular ornithine.

Figure 2. Cellular GABA is produced from extracellular ornithine.

a. GABA synthesis pathways. **b.** $^{13}C_5$-Glutamine tracing experiment and cellular levels of $^{13}C_5$-Glutamine, $^{13}C_5$-Glutamate and $^{13}C_4$-GABA. **c.** $^{13}C_6$-Arginine tracing experiment and cellular levels of $^{13}C_6$-Arginine, $^{13}C_5$-Ornithine and $^{13}C_4$-GABA after 13C6-Arginine tracing experiment. **d.** Relative quantification of extracellular ornithine production in fresh RPMI media (Ctr, empty circles) or containing 10% fetal bovine serum (Serum, full circles). **e.** Ornithine levels after 24h in RPMI media containing 10% of control fetal bovine serum (Control FBS) or after heat-inactivation (Heated FBS). **f.** Simultaneous labeling of GABA from 1.15 mM $^{13}C_6$ arginine and 0.2 mM $^2H_6$ ornithine in A549 cells cultured heat-inactivated dialyzed FBS. **g.** Cellular $^2H_6$-GABA levels in HepG2 cells overexpressing empty vector (Ctr) or SLC45A4 and cultured with 10% hiFBS and 0.2 mM $^2H_6$ ornithine. In all figures, data are mean ± SEM; n represents biologically independent replicates. **P<0.01; *P<0.05; ns, not significant by two-sided Student's t-test.

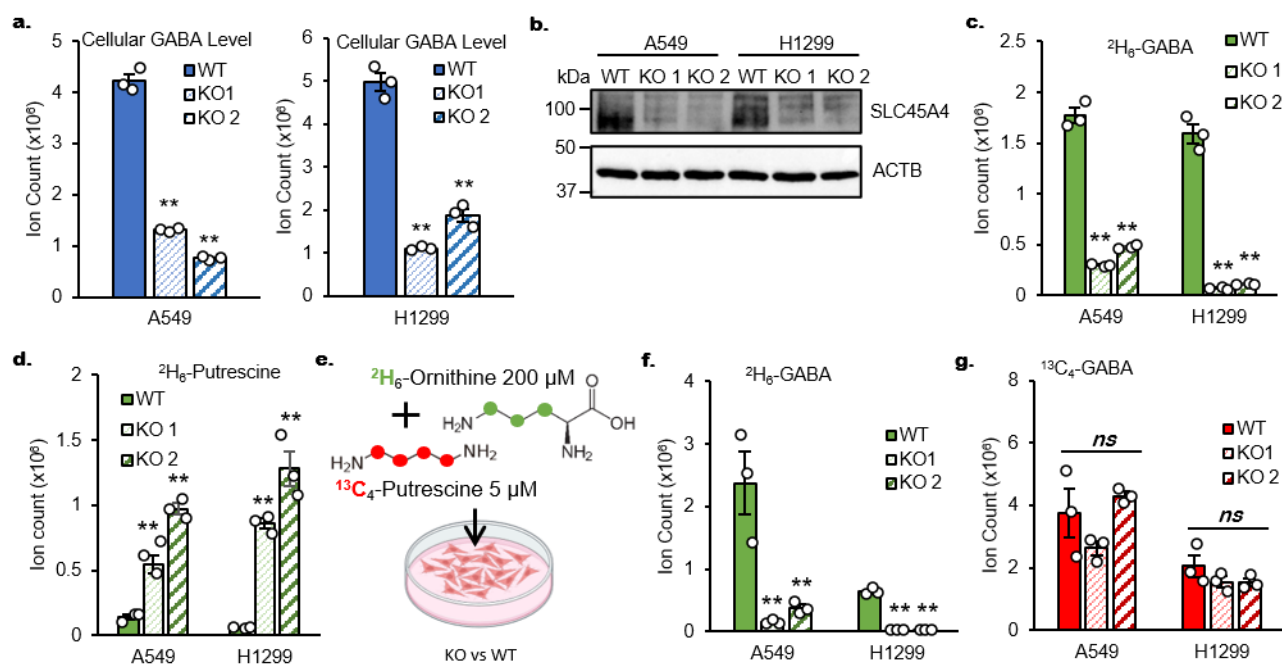Figure 3. GABA production from ornithine and putrescine is differentially regulated by SLC45A4.

Figure 3. GABA production from ornithine and putrescine is differentially regulated by SLC45A4.
a. Cellular level of GABA in A549 and H1299 Wild-type (WT) and their 2 homozygotes generated SLC45A4-knockouts (KO1 & KO2). **b.** SLC45A4 protein expression in A549 and H1299 WT and KOs cells. **c.d.** Cellular level of GABA (**c.**) and Putrescine (**d.**) derived from $^2H_6$-ornithine in A549 and H1299 WT and KO cells. **e.** Schematic of $^2H_6$-ornithine and $^{13}C_4$-putrescine dual-tracing experiment. **f.g.** Cellular level of GABA derived from **f.** $^2H_6$-ornithine ($^2H_6$-GABA) and from **g.** $^{13}C_4$-putrescine ($^{13}C_4$-GABA) in dual-tracing experiment. In all figures, data are mean ± SEM.; n represents biologically independent replicates. **P<0.01; *P<0.05; ns, not significant by two-sided Student's t-test or two-way ANOVA followed by Tukey's post-hoc test for dual-tracing experiment (f. and g.).

10

Figure 4. GABA synthesis depends on the activity of ornithine decarboxylase and diamine oxidases.
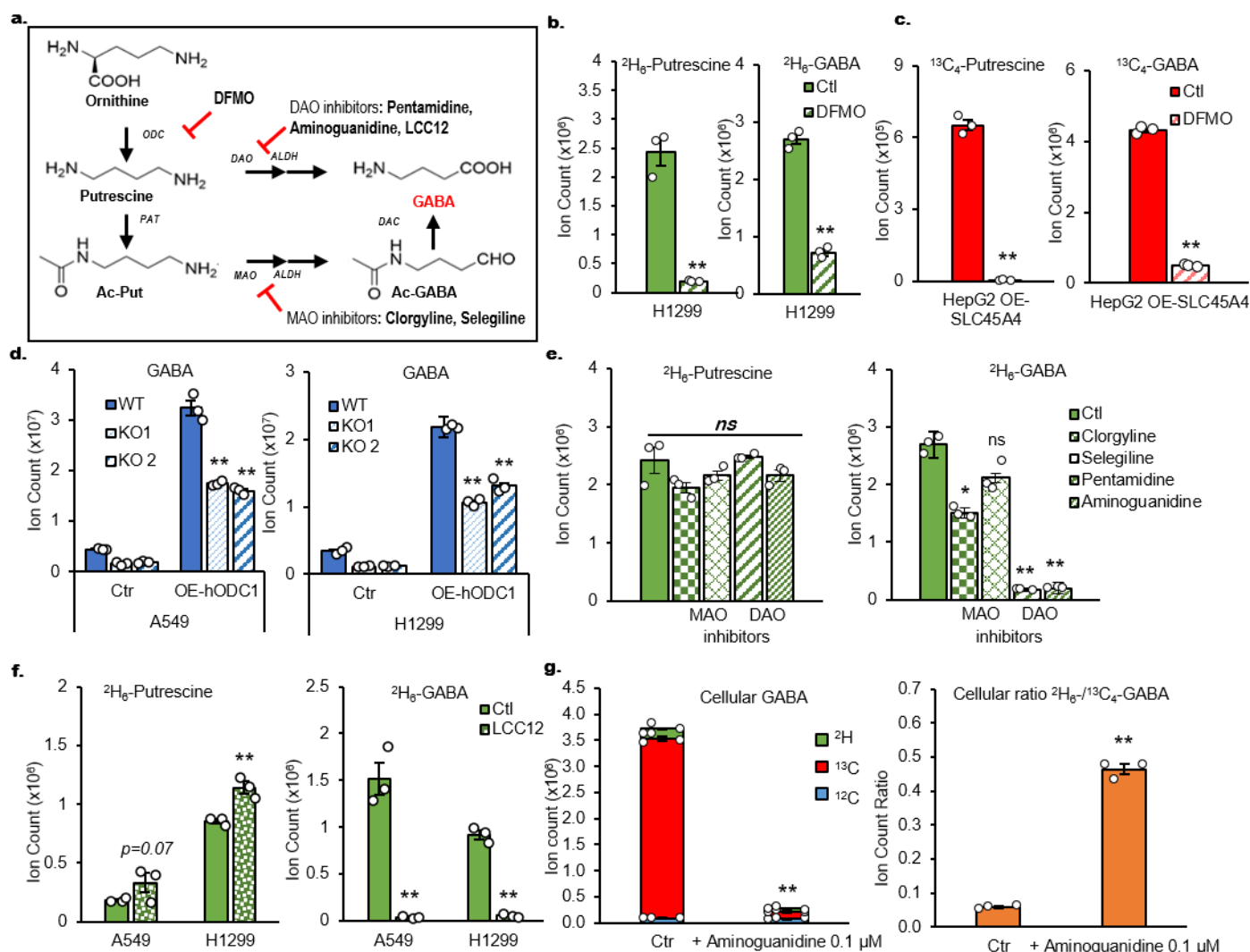

Figure 4. GABA synthesis depends on the activity of ornithine decarboxylase and diamine oxidases.
a. Inhibition of GABA synthesis by DFMO or Monoamine Oxidases/Diamine Oxidases (MAO/DAO) inhibitors. **b.c.** Cellular level of Putrescine (left) and GABA (right) after 24h treatment with ODC1-inhibitor DFMO in **b.** H1299 culture with $^2H_6$-Ornithine and **c.** HepG2 overexpressing SLC45A4 cultured with $^{13}C_6$-Arginine. **d.** Cellular level of GABA in A549 (left) and H1299 (right) WT and their SLC45A4-KO cells (KO1 & KO2) overexpressing empty vector (Ctr) or human-ODC1 (OE-hODC1). **e.** Cellular level of putrescine (left, $^2H_6$-putrescine) and GABA (right, $^2H_6$-GABA) in H1299 cells cultured with $^2H_6$-Ornithine and treated with 0 μM (Ctr) or MAO inhibitors Clorgyline (5 μM) or Selegiline (10 μM) or DAO inhibitors Pentamidine (1 μM) or Aminoguanidine (0.1 μM). **f.** Cellular level of putrescine (left, $^2H_6$-putrescine) and GABA (right, $^2H_6$-GABA) in H1299 cells cultured with $^2H_6$-Ornithine and treated with 0 mM (Ctr) or 10 μM of mitochondrial Copper(II) chelator LCC12. **g.** Fractions of cellular GABA in A549 WT cells supplemented with $^2H_6$-Ornithine and $^{13}C_4$-Putrescine in absence (Ctr) or presence of 0.1 μM of aminoguanidine. In all figures, data are mean ± SEM.; n represents biologically independent replicates. **P<0.01; *P<0.05; ns, not significant by two-sided Student's t-test.

11

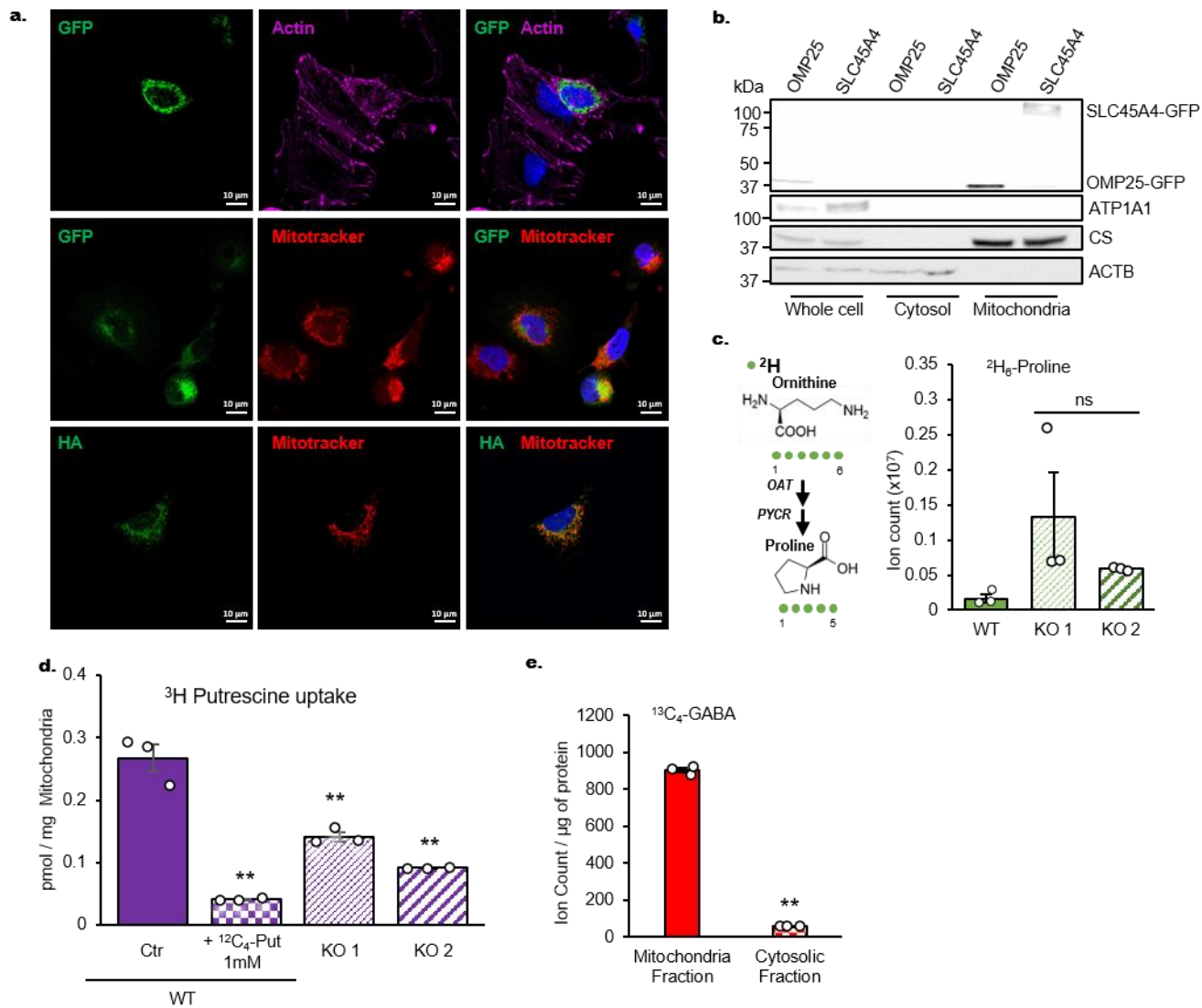Figure 5. SLC45A4 encodes a mitochondrial putrescine transporter.

Figure 5. SLC45A4 encodes a mitochondrial putrescine transporter.

a. Immunofluorescent detection of SLC45A4 subcellular localization. A549 cells transiently express SLC45A4-GFP (top and middle panels) or stably overexpress 3HA tagged SLC45A4 protein (bottom panel) and stained for HA, plasma membrane marker (Actin) or mitochondrial marker (MitoTracker™). HA epitope, green; organelle markers, red. **b.** SDS-PAGE of whole cell, cytosol and mitochondria fractions from HEK293T cells transiently transfected with cDNA encoding GFP tagged OMP25 or SLC45A4. OMP25 and SLC45A4 were detected by GFP antibody. Markers of plasma membrane (ATP1A1), mitochondria (CS) and cytosol (ACTB) were also probed. **c.** Proline labeling pattern after $^2H_6$-ornithine tracing experiment. **d.** Competitive uptake assay in isolated mitochondria from A549 cells using radiotracer ^3H-Putrescine alone (Ctr, KO 1 and KO 2) or in combination with 1 mM of cold $^{12}C_4$-Putrescine. **e.** $^{13}C_4$-GABA level derived from $^{13}C_4$-putrescine after 1h incubation in isolated mitochondria (Mitochondria Fraction) or in isolated cytosol (Cytosolic Fraction) from A549 cells. In all figures, data are mean ± SEM; n represents biologically independent replicates. **P<0.01; *P<0.05; ns, not significant by two-sided Student's t-test.

12

METHODS

Metabolomic-Transcriptomic association calculation

The metabolomics and transcriptomic profiles of 898 cancer cell lines were downloaded from the Cancer Cell Line Encyclopaedia (CCLE)[1] portal (https://portals.broadinstitute.org/ccle). For each pair of gene and metabolites, a linear regression model was applied to evaluate the association in the 898 cell lines. The T statistics (t-stat) and P value were calculated.

Cell culturing

A549, H1299 and HepG2 cells were purchased from American Type Culture Collection (ATCC). The HEK293T cells were a gift from Dr. Weixing Zong of Rutgers University. A549 and H1299 cell lines were cultured in RPMI 1640 media (Gibco, 11875135), HepG2 and HEK293T in DMEM media (ATCC, 30-2003); all media are supplemented with 10% FBS (Gibco, 26140079) and 1% Penicillin-Streptomycin (Gibco, 15140122). When appropriate, the FBS was substituted with dialysed FBS (Gibco, A3382001) heat-inactivated 70 °C for 1 hour. For isotope labeling experiments that required to substitute arginine or glutamine with U-^{13}C isotopologues, the corresponding substances were supplemented to SILAC RPMI 1640 Flex Media (Gibco, A2494201) to match the same formula as ordinary RPMI 1640 (*See **Stable Isotope Tracing** section*). All cell lines grown in standard cell culture conditions (37 °C, 5% CO_2) and were free of microbial contamination, including mycoplasma. Cells were passaged twice a week and used between passages 10 to 20.

Expression plasmids

Human cDNA encoding SLC45A4 (NCBI: NM_001286646.1) was purchased from GenScript. The DNA sequence of SLC45A4 was cloned to pLPC-N FLAG vector (Addgene, 12521) using BamHI-HF (NEB, R3136S) and EcoRI-HF (NEB, R3101S) restriction digestion and Quick Ligation Kit (NEB, M2200S). Sequences coding 3×HA or 3×HA-GFP tags were added to the C-terminal of the protein using gene-specific PCR and HiFi assembly (NEB). The 3×HA and 3×HA-GFP sequences were cloned from pMXs-3XHA-EGFP-OMP25 plasmid (Addgene 83356).

Human cDNA encoding ODC1 (NCBI: NM_002539.3) was purchased from GenScript with eGFP cloned at the C-terminal in the vector pDCNA3.1.

Transient Overexpression

Cells were seeded in new 12-well plates at the density of 2×10^5 / ml. When the cells reached about 70% confluence, cells were transfected with Lipofectamine 3000 according to manufacturer's instructions (Invitrogen, L3000015). 1 µg expression vector plasmid DNA was first mixed with 2 µl P3000 reagent in 50 µl Opti-MEM reduced serum medium (Gibco, 31985070), then mixed with 3 µl Lipofectamine 3000 in another 50 µl Opti-MEM. The mixture was incubated at room temperature for 15 min and added directly to the cell culture. 24h later, the media were replaced with the one containing stable isotope tracers if necessary.

Retroviral production and transduction

HEK293T cells were seeded in new T-75 flask at the density of 2×10^5 / ml. When the cells reached about 70% confluence, cells were transfected with Lipofectamine 3000 ((Invitrogen, L3000015) according to manufacturer's instructions. 15 µg expression vector plasmid, 9 µg pUMVC plasmid (Addgene, 8449), and 3 µg pCMV-VSV-G plasmid (Addgene, 8454) was used for each transfection. The plasmid DNA was first mixed with 40 µl P3000 in 750 µl Opti-MEM reduced serum medium (Gibco, 31985070), then mixed with 59 µl Lipofectamine 3000 in another 750 µl Opti-MEM. The mixture was incubated at room temperature for 15 min and added directly to the cell culture. The culture media were refreshed with normal DMEM with 10% FBS and 1x Penicillin-Streptomycin after 6h. 24h and 48h after transfection, media were collected, centrifuged for 5 min at $1000 \times$ g and filtered using a 0.45 µm filter. The titer of virus was measured using the qPCR Retrovirus Titer Kit (ABM, G949). If the titer

was less than 2×10^6 IU/ml, the virus media was concentrated using the Retro-X Concentrator (Takara, 631455) to reach 2×10^6 IU/ml. The virus media was aliquoted and stored at -80 ˚C. Cells to be transduced were seeded at the density of 2×10^5 / ml. When the cells reached about 50% confluence, conditioned media with virus was mixed with normal cell media with Multiplicity Of Infection (MOI) 1:1 ratio and supplemented with 10 ug/ml polybrene infection transfection reagent (Sigma, TR-1003-G . The mixture with appropriate volume was added to the cell three times with 12-18h interval. After 7 days, cells were sorted for GFP$^+$ if necessary.

siRNA knockdown

A549 or H1299 cells were seeded in 6-well plates at the density of 2×10^5 / ml. When the cells reached about 70% confluence, cells were transfected with siRNA Transfection Reagent (Santa Cruz Biotechnology, sc-29528) according to manufacturer's instructions. siRNAs targeting human SLC45A4 (SCBT, sc-77846) and non-targeting Scramble controls (SCBT, sc-37007) were obtained from SCBT and re-suspended at 10 µM in RNAse free water. 4 µl siRNA (20 nM) was first mixed with 100 µl Opti-MEM (Gibco, 31985070), then mixed with 4 µl siRNA Transfection Reagent in another 100 µl Opti-MEM. The mixture was incubated at room temperature for 30 min and mixed with 800 µl Opti-MEM. Cells were washed once with 2 ml Opti-MEM, then covered with 1 ml siRNA mixture and incubated for 6 hours at 37 °C, 5% CO_2. After the incubation, 1 ml of RPMI 1640 media with 20% FBS and 2× Penicillin-Streptomycin were added. Media was replaced the next day with the one containing stable isotope tracers if necessary.

Construction of stable SLC45A4 knock down and knock off cell lines

CRISPR/Cas9 was used to interfere single (knock-down) or double allele (knockout) of SLC45A4 genomic sequence by the Genome Editing Core Facility of Cancer Institute of New Jersey.

Stable Isotope Tracing

Cells were seeded in new 12-well plates at the density of 2×10^5 / ml. When the cells reached about 70% confluence, the media was replaced with SILAC RPMI 1640 Flex Media (Gibco, A2494201) supplemented with 11.11 mM D-glucose or, 0.22 mM L-lysine, 2.05 mM L-glutamine or $^{13}C_5$-glutamine (CLM-1822-H), 1.15 mM L-arginine or $^{13}C_6$-arginine (CLM-2265-H), 10% FBS and 1x Penicillin-Streptomycin. When appropriate, the following substrates were also added: 200 µM $^2H_6$-ornithine (DLM-2969), 20 µM $^{13}C_4$-putrescine (CLM-6574) and 20 µM GABA or $^{13}C_4$-GABA (CLM-8666). For subsequent labeling experiments involved $^2H_6$ ornithine, FBS was substituted with iFBS and 200 µM $^2H_6$-ornithine were added. All cells were cultured with isotope tracers for 24 h and metabolite extraction was performed.

Mitochondria Isolation

For western analysis, the mitochondria were isolated using Minute Mitochondria Isolation Kit (Invent Biotechnology, Minute™ Mitochondria Isolation Kit, MP-007). 4×10^7 HEK293T cells that transiently overexpressing SLC45A4-GFP or OMP25-GFP were collected by trypsinization. Cells were washed once with 1 ml cold PBS, re-suspended in 250 µl buffer A and incubated on ice for 10 min followed by vigorous vortex for 30 s. The lysate was then transferred to a filter cartridge and centrifuged at $16,000 \times$ g for 30 seconds. The flow-through were vortexed and re-passed the same cartridge one more time. The flow-through were vortexed and centrifuged at $700 \times$ g for 1 min. The supernatant was transferred to a new 1.5 ml tube and mixed with 300 µl buffer B by vortexing for 10 s. The mixture was centrifuged at $16,000 \times$ g for 30 min and the resulting pellet was re-suspended in 200 µl buffer B and vigorously vortexed for 20 s. The mixture was centrifuged at $8,000 \times$ g for 5 min and the supernatant was transferred to a new 2 ml tube. 1.6 ml cold PBS was added to the tube and the mixture was centrifuged at $16,000 \times$ g for 30 min. The resulting mitochondria pellet were stored at -80°C until analysis.

For metabolomics analysis, 20×10^6 A549 cells stably expressing OMP25-3HA-GFP protein (PMID: 27565352) (retrovirus transduced) were collected by trypsinization. Cells were washed once with cold PBS and re-suspended in 250 µl buffer A (Invent Biotechnology, Minute™ Mitochondria Isolation Kit, MP-007) and incubated on ice for 10 min followed by vigorous vortex for 30 s. The lysate was transferred to a glass homogenizer and subjected to 20 strokes to ensure plasma membrane disruption. Resulting lysate was then transferred to a filter cartridge (Invent Biotechnology, Minute™ Mitochondria Isolation Kit, MP-007) and centrifuged at $16,000 \times g$ for 30 seconds. The pellet was re-suspended by gently vortexing and centrifuged at $700 \times g$ for 1 min. The Post-Nuclear Supernatant (PNS) obtained was transferred to a new tube and mixed with 200 µl Pierce™ anti-HA magnetic beads (Thermo Scientific, 88837) previously washed three times with KPBS (136 mM KCl, 10 mM KH_2PO_4, pH 7.25). The mixture was incubated at 4°C on an end-over-end rotator for 30 min. During the incubation, the mitochondria/beads were further mixed every 10 min by pipetting to avoid aggregation of the beads. After the incubation, magnet was applied to separate the mitochondria/beads from the cytosolic fraction which was preserved in a separate tube. The mitochondria/beads were gently washed 3 times with 1 ml KPBS and ready for the further analysis.

$^{13}C_4$-Putrescine incubation in isolated mitochondria

Mitochondria and cytosolic fraction isolated from A549 stably expressing OMP25-3HA-GFP as previously described were incubated for 1h at 37°C 5% CO2 with 1 mM of $^{13}C_4$-putrescine: isolated mitochondria on beads were incubated on KPBS containing the $^{13}C_4$-putrescine while $^{13}C_4$-putrescine was spiked into the cytosolic fraction suspension. After the incubation, magnet was applied to separate the mitochondria/beads from the incubation media which was preserved in a separate tube. The beads were gently washed 3 times with 1 ml KPBS and ready for the further analysis.

^3H uptake assay

Mitochondria were isolated from 50×10^6 A549 cells using sub cellular fractionation method described in the "For western analysis" section of Mitochondrial Isolation. Mitochondria were kept on ice at all times until the assay. Pellets obtained after the last centrifugation ($16,000 \times g$ for 30 min) were re-suspended in mitochondrial isolation buffer (MIB: 0.25 M sucrose, 10 mM TRIS, 1 mM EGTA, pH 7.4). ^3H putrescine (1 µl at 0.1 mCi/ml, 55 mCi/mmol) was added to each mitochondria suspensions and were incubated at 37 °C for 30 min on a heat block. Following incubation, the mitochondria suspensions were spun down at 13,000 x g for 10 minutes and the supernatant was discarded. The mitochondrial pellets were then washed 3 times with 1 ml of MIB and centrifuged 10min at 13,000 x g. After washing, pellets were resuspended in 1 ml MIB each. 300 µl was taken from each sample to a liquid scintillation vial containing 10 ml of scintillation fluid. The scintillation vials were capped tight, briefly vortexed and counted for 1 min.

Metabolite Extraction

For whole cell metabolite extraction, $0.5.10^6$ cells in the culture were washed twice with PBS and extracted with 0.5 ml ice cold 40:40:20 (methanol:acetonitrile:water) solution with 0.5% formic acid. The cells were scraped off the plate followed by incubation on ice for 10 min, and neutralized by the addition of 25 µl 15% (m/v) NH_4HCO_3 solution. The extracts were transferred to a 1.5 ml tube. For conditioned media metabolite extraction, 5 µl of culture media was mixed with 500 µl of ice cold 40:40:20 (methanol:acetonitrile:water) solution with 0.5% formic acid and neutralized by the addition of 25 µl 15% (m/v) NH_4HCO_3 solution. For mitochondrial metabolite extraction, 200 µl ice cold 40:40:20 solution with 0.5% formic acid was directly added to the magnetic beads, followed by incubation on ice for 10 min, and neutralized by the addition of 10 µl 15% (m/v) NH_4HCO_3 solution. 80 µl of cytosolic fraction was mixed with 320 µl ice cold 1:1 (methanol:acetonitrile) followed by incubation on ice for 10 min, and neutralized by the addition of 20 µl 15% (m/v) NH_4HCO_3 solution. The whole cell or

15

mitochondrial or cytosolic metabolite extracts were then centrifuged at 4°C and 16,000 × g for 10 min and transferred to a clean tube and stored at -80°C until analysis. Mitochondrial and cytosolic fraction metabolite extracts were cleaned with Phree™ Phospholipid Removal column (Phenomenex, 8B-S133-TAK) for 5 min at 1,000g before vialed for LC-MS analysis.

Metabolomic LC-MS Analysis

HILIC separation was performed on a Vanquish Horizon UHPLC system (ThermoFisher) with an XBridge BEH Amide column (150 mm × 2.1 mm, 2.5 µm particle size, Waters) using a gradient of solvent A (95%:5% H2O:acetonitrile with 20 mM acetic acid, 40 mM ammonium hydroxide, pH 9.4) and solvent B (20%:80% H2O:acetonitrile with 20 mM acetic acid, 40 mM ammonium hydroxide, pH 9.4). The gradient was 0 min, 100% B; 3 min, 100% B; 3.2 min, 90% B; 6.2 min, 90% B; 6.5 min, 80% B; 10.5 min, 80% B; 10.7 min, 70% B; 13.5 min, 70% B; 13.7 min, 45% B; 16 min, 45% B; 16.5 min, 100% B; and 22 min, 100% B. The flow rate was 300 µl/min with 5 µl injection volume. The column temperature was 25 °C and the autosampler temperature was 4 °C. MS scans were obtained in both negative and positive ion modes with a resolution of 70,000 at m/z 200, in addition to an automatic gain control target of 3×10^6 and m/z scan range of 72 to 1000. Metabolite data was obtained using the MAVEN software package[10] (mass accuracy window: 15 ppm). All isotope natural abundance correction were done using AccuCor2 **(PMID: 34193963)**.

Immunofluorescence

A549 cells transiently overexpressing SLC45A4-C-eGFP or stably SLC45A4-3HA were seeded on poly-lysine coated glass coverslips (Neuvitro, GG18PLL) at the density of 2×10^5 / ml. When the cells reached about 70% confluence, cells were incubated with 100 nM MitoTracker Red CMXRos (Invitrogen, M7512) at 37 °C for 30 min when appropriate. After two PBS washes, cells were fixed using 4% paraformaldehyde (Thermo Scientific Chemicals, J61899.AK) in PBS for 15 min at room temperature. Fixed cells were then washed three times in PBS, permeabilized with Triton X-100 0.2% in PBS 1X for 20 min and blocked in PBS 1X containing 2% Normal Goat Serum (Invitrogen, 31873), 0.02% Triton X-100, 0.1% BSA for 30 min at room temperature (Blocking buffer). Primary Mouse anti-HA antibody (CST, 2367, 1:800) was diluted in blocking buffer and incubated with cells overnight at 4 °C. After washing twice with TBS Tween-20 0.1% and once with blocking buffer, secondary antibodies were diluted in blocking buffer and incubated with cells for 1 h at room temperature in dark. Goat anti-Mouse IgG–Alexa Fluor 488 (CST 4408, 1:500); Alexa Fluor 647 Phalloidin (Invitrogen, A22287, 1:600) were used when appropriate. Cells were washed three times with PBS containing 0.2% Triton X-100. Coverslip were mounted with Fluoroshield with DAPI (Sigma, F6057). Images were obtained using a LSM-700 confocal microscope setup that includes 405, 488 and 555 nm lasers and 63× objective. Image analysis was performed on ZEN 3.6 software (Zeiss).

RNA Analysis

Total RNA was obtained from cell culture using the RNeasy Plus Mini Kit (Qiagen, 74004) following supplier instructions. Complementary DNA (cDNA) was generated from 1 µg total RNA using the iScript cDNA Synthesis kit (Bio-Rad, 1708841). Primers were designed with NCBI Primer-BLAST. The primer sequences for detecting *SLC45A4* are 5'-GATGGCCATGTTTCCCAACG-3'(forward) and 5'-GGCTGTGGTGGATGTACTGC-3' (reverse). The primer sequences for detecting *ACTB* are 5'- GACCTGACTGACTACCTCAT-3'(forward) and 5'-TCTCCTTAATGTCACGCACG-3' (reverse) Quantitative PCR (qPCR) reactions were conducted using the SYBR green PCR master mix (Bio-Rad, 1725121) in CFX96 Touch Real-Time PCR Detection System (Bio-Rad). CT values were normalized to *ACTB* mRNA and interpreted as fold changes to the Ctr or WT cell group.

Protein Extraction and Western Blotting

One million cells were washed once with PBS and extracted with 100 ul protein extraction RIPA buffer and protease inhibitors from Santa Cruz Biotechnology (SCTB, sc-24948). The extracts were incubated 10 min on ice and sonicated 5 s for three times. The sonicated extracts were mixed with $2\times$ Laemmli loading dye containing 5% 2-mercaptoethanol and incubated at room temperature for 10 min without boiling. 10 ug of protein samples were loaded per lane and electrophoresed on 7.5% Mini-PROTEAN® TGX™ Precast Protein Gels (BioRad, 4561025) and transferred to 0.2 μm nitrocellulose membrane using semi dry transfer system (BioRad). Membranes were incubated with blocking buffer (5% milk in Tris-buffered saline (TBS) pH 7.6 containing 0.1% (v/v) Tween-20 (TBST)) for 1h at room temperature and incubated with primary antibodies at 4 °C overnight. Primary antibodies were diluted in the blocking buffer: GFP (CST 2956, 1:1000); ATP1A1 (CST 3010, 1:1000); Citrate Synthase (CS) (CST 14309, 1:1000); β-Actin (ACTB) (CST 4967, 1:1000); SLC45A4 (Genescript R11554, 1:3000); CYPB (CST 43603, 1:1000). After three washes with TBST, membranes were incubated 1h at room temperature with the anti-rabbit secondary antibody diluted in blocking buffer (CST 7074, 1:2000). After three washes with TBST, membranes were incubated with HRP substrate (Millipore 221543) and imaged using ChemiDoc touch imaging system (Bio-Rad).

Statistical Analysis

Statistical analyses were performed using Excel 2016 for Student's t-test and R/R-Studio for ANOVA.

Data and Code availability

All data and computer code are available from the authors upon reasonable request.

Author contributions X.S. conceived this project. C.C., Y.W., and X.S. designed the study. C.C, Y.W., J.A., X.S. performed experiments and data analyses. X.S. supervised the whole study. C.C., Y.W. and X.S. wrote the original and revised manuscript.

Competing interests The authors declare no competing interests.

Correspondence and requests for materials should be addressed to X.S.

References

1. Kell, D. B., Dobson, P. D. & Oliver, S. G. Pharmaceutical drug transport: The issues and the implications that it is essentially carrier-mediated only. *Drug Discovery Today* vol. 16 704–714 (2011).

2. Kell, D. B. & Oliver, S. G. How drugs get into cells: tested and testable predictions to help discriminate between transporter-mediated uptake and lipoidal bilayer diffusion. *Front. Pharmacol.* **5**, 231 (2014).

3. Pizzagalli, M. D., Bensimon, A. & Superti-Furga, G. A guide to plasma membrane solute carrier proteins. *FEBS J.* **288**, 2784–2835 (2021).

4. Höglund, P. J., Nordström, K. J. V., Schiöth, H. B. & Fredriksson, R. The Solute Carrier Families Have a Remarkably Long Evolutionary History with the Majority of the Human Families Present before Divergence of Bilaterian Species. *Mol. Biol. Evol.* **28**, 1531–1541 (2011).

5. Hediger, M. A. *et al.* The ABCs of solute carriers: Physiological, pathological and therapeutic implications of human membrane transport proteins. *Pflugers Arch. Eur. J. Physiol.* **447**, 465–468 (2004).

6. Hediger, M. A., Clémençon, B., Burrier, R. E. & Bruford, E. A. The ABCs of membrane transporters in health and disease (SLC series): Introduction. *Molecular Aspects of Medicine* vol. 34 95–107 (2013).

7. Schlessinger, A. *et al.* Comparison of human solute carriers. *Protein Sci.* **19**, 412–428 (2010).

8. Ferrada, E. & Superti-Furga, G. A structure and evolutionary-based classification of solute carriers. *iScience* **25**, 105096 (2022).

9. Williams, A. J. *et al.* Open PHACTS: semantic interoperability for drug discovery. *Drug Discov. Today* **17**, 1188–1198 (2012).

10. Wang, W. W., Gallo, L., Jadhav, A., Hawkins, R. & Parker, C. G. The Druggability of Solute Carriers. *J. Med. Chem.* **63**, 3834–3867 (2020).

11. Lin, L., Yee, S. W., Kim, R. B. & Giacomini, K. M. SLC transporters as therapeutic targets: Emerging opportunities. *Nature Reviews Drug Discovery* vol. 14 543–560 (2015).

12. Giacomini, K. M. *et al.* New and Emerging Research on Solute Carrier and ATP Binding Cassette Transporters in Drug Discovery and Development: Outlook From the International Transporter Consortium. *Clin. Pharmacol. Ther.* **112**, 540–561 (2022).

13. Bartölke, R., Heinisch, J. J., Wieczorek, H. & Vitavska, O. Proton-associated sucrose transport of mammalian solute carrier family 45: an analysis in Saccharomyces cerevisiae. *Biochem. J.* **464**, 193–201 (2014).

14. Meixner, E. *et al.* A substrate-based ontology for human solute carriers. *Mol. Syst. Biol.* **16**, 9652 (2020).

15. Zheng, D., Wei, Z. & Guo, W. Identification of a Solute Carrier Family-Based Signature for Predicting Overall Survival in Osteosarcoma. *Front. Genet.* **13**, 896 (2022).

16. Chen, W. *et al.* SLC45A4 promotes glycolysis and prevents AMPK/ULK1-induced autophagy in TP53 mutant pancreatic ductal adenocarcinoma. *J. Gene Med.* (2021) doi:10.1002/jgm.3364.

17. Awapara, J., Landua, A. J., Fuerst, R. & Seale, B. FREE γ-AMINOBUTYRIC ACID IN BRAIN. *J. Biol. Chem.* **187**, 35–39 (1950).

18. ROBERTS, E. & FRANKEL, S. γ-AMINOBUTYRIC ACID IN BRAIN: ITS FORMATION FROM GLUTAMIC ACID. *J. Biol. Chem.* **187**, 55–63 (1950).

19. Gladkevich, A., Korf, J., Hakobyan, V. P. & Melkonyan, K. V. The peripheral GABAergic system as a target in endocrine disorders. *Autonomic Neuroscience: Basic and Clinical* vol. 124 1–8 (2006).

20. Young, S. Z. & Bordey, A. GABA's control of stem and cancer cell proliferation in adult neural and peripheral niches. *Physiology* **24**, 171–185 (2009).

21. Dahn, M. L. *et al.* Metabolite profiling reveals a connection between aldehyde dehydrogenase 1A3 and GABA metabolism in breast cancer metastasis. *Metabolomics* **18**, (2022).

22. Erlander, M. G., Tillakaratne, N. J. K., Feldblum, S., Patel, N. & Tobin, A. J. Two genes encode distinct glutamate decarboxylases. *Neuron* **7**, 91–100 (1991).

23. Seiler, N. On the role of GABA in vertebrate polyamine metabolism. *Physiological chemistry and physics* vol. 12 411–429 (1980).

24. Caron, P. C., Kremzner, L. T. & Cote, L. J. GABA and its relationship to putrescine metabolism in the rat brain and pancreas. *Neurochem. Int.* **10**, 219–229 (1987).

25. Tsuji, M. & Nakajima, T. Studies on the Formation of γ-Aminobutyric Acid from Putrescine in Rat

Organs and Purification of Its Synthetic Enzyme from Rat Intestine. *J. Biochem.* **83**, 1407–1412 (1978).

26. Fogel, W. A., Bieganski, T., Schayer, R. W. & Maslinski, C. Involvement of diamine oxidase in catabolism of14C-putrescine in mice in vivo with special reference to the formation of γ-aminobutyric acid. *Agents Actions* **11**, 679–684 (1981).

27. Seiler, N. & Al Therib, M. J. Putrescine catabolism in mammalian brain. *Biochem. J.* **144**, 29–35 (1974).

28. Yoon, B. E. *et al.* Glial GABA, synthesized by monoamine oxidase B, mediates tonic inhibition. *J. Physiol.* **592**, 4951–4968 (2014).

29. Kurys, G., Ambroziak, W. & Pietruszko, R. Human aldehyde dehydrogenase: Purification and characterization of a third isozyme with low Km for γ-aminobutyraldehyde. *J. Biol. Chem.* **264**, 4715–4721 (1989).

30. Ambroziak, W. & Pietruszko, R. Human aldehyde dehydrogenase. Activity with aldehyde metabolites of monoamines, diamines, and polyamines. *J. Biol. Chem.* **266**, 13011–13018 (1991).

31. Kim, J. I. *et al.* Aldehyde dehydrogenase 1a1 mediates a GABA synthesis pathway in midbrain dopaminergic neurons. *Science (80-.).* **350**, 102–106 (2015).

32. Ghandi, M. *et al.* Next-generation characterization of the Cancer Cell Line Encyclopedia. *Nature* **569**, 503–508 (2019).

33. Li, H. *et al.* The landscape of cancer cell line metabolism. *Nat. Med.* **25**, 850–860 (2019).

34. Gregor, P., Russel Nash, S., Caron, M. G., Seldin, M. F. & Warren, S. T. Assignment of the creatine transporter gene (SLC6A8) to human chromosome Xq28 telomeric to G6PD. *Genomics* **25**, 332–333 (1995).

35. Nezu, J. I. *et al.* Primary systemic carnitine deficiency is caused by mutations in a gene encoding sodium ion-dependent carnitine transporter. *Nat. Genet.* **21**, 91–94 (1999).

36. Anderson, C. M. H., Howard, A., Walters, J. R. F., Ganapathy, V. & Thwaites, D. T. Taurine uptake across the human intestinal brush-border membrane is via two transporters: H+-coupled PAT1 (SLC36A1) and Na+- and Cl−-dependent TauT (SLC6A6). *J. Physiol.* **587**, 731–744 (2009).

37. Kovács, Z. *et al.* Critical Role of Astrocytic Polyamine and GABA Metabolism in Epileptogenesis. *Front. Cell. Neurosci.* **15**, 787319 (2022).

38. Sullivan, M. R. *et al.* Quantification of microenvironmental metabolites in murine cancers reveals determinants of tumor nutrient availability. *Elife* **8**, (2019).

39. Shore, P. A. & Cohn, V. H. Comparative effects of monoamine oxidase inhibitors on monoamine oxidase and diamine oxidase. *Biochem. Pharmacol.* **5**, 91–95 (1960).

40. McGrath, A. P. *et al.* Structure and inhibition of human diamine oxidase. *Biochemistry* **48**, 9810–9822 (2009).

41. Johnston, J. P. Some observations upon a new inhibitor of monoamine oxidase in brain tissue. *Biochem. Pharmacol.* **17**, 1285–1297 (1968).

42. Tandarić, T. & Vianello, R. Computational Insight into the Mechanism of the Irreversible Inhibition of Monoamine Oxidase Enzymes by the Antiparkinsonian Propargylamine Inhibitors Rasagiline and Selegiline. *ACS Chem. Neurosci.* **10**, 3532–3542 (2019).

43. Ostadkarampour, M. & Putnins, E. E. Monoamine Oxidase Inhibitors: A Review of Their Anti-Inflammatory Therapeutic Potential and Mechanisms of Action. *Front. Pharmacol.* **12**, 676239 (2021).

44. Solier, S. *et al.* A druggable copper-signalling pathway that drives inflammation. *Nature* **617**, 386–394 (2023).

45. TABOR, C. W., TABOR, H. & ROSENTHAL, S. M. Purification of amine oxidase from beef plasma. *J. Biol. Chem.* **208**, 645–661 (1954).

46. De Matteis, G., Agostinelli, E., Mondovì, B. & Morpurgo, L. The metal function in the reactions of bovine serum amine oxidase with substrates and hydrazine inhibitors. *J. Biol. Inorg. Chem.* **4**, 348–353 (1999).

47. Ruprecht, J. J. & Kunji, E. R. S. The SLC25 Mitochondrial Carrier Family: Structure and Mechanism. *Trends Biochem. Sci.* **45**, 244–258 (2020).

48. Hadley, B. *et al.* Nucleotide Sugar Transporter SLC35 Family Structure and Function. *Comput. Struct. Biotechnol. J.* **17**, 1123–1134 (2019).

49. Le, L. *et al.* SLC45A2 protein stability and regulation of melanosome pH determine melanocyte

pigmentation. *Mol. Biol. Cell* **31**, 2687–2702 (2020).

50. Liu, Y. *et al.* Ablation of H+/glucose Exporter SLC45A2 Enhances Melanosomal Glycolysis to Inhibit Melanin Biosynthesis and Promote Melanoma Metastasis. *J. Invest. Dermatol.* (2022) doi:10.1016/J.JID.2022.04.008.

51. Camacho, J. A. *et al.* Hyperornithinaemia-hyperammonaemia-homocitrullinuria syndrome is caused by mutations in a gene encoding a mitochondrial ornithine transporter. *Nat. Genet.* **22**, 151–158 (1999).

52. Toninello, A., Dalla Via, L., Siliprandi, D. & Garlid, K. D. Evidence that spermine, spermidine, and putrescine are transported electrophoretically in mitochondria by a specific polyamine uniporter. *J. Biol. Chem.* **267**, 18393–18397 (1992).

53. Ginguay, A., Cynober, L., Curis, E. & Nicolis, I. Ornithine Aminotransferase, an Important Glutamate-Metabolizing Enzyme at the Crossroads of Multiple Metabolic Pathways. *Biology (Basel).* **6**, (2017).

54. Ding, J. *et al.* Human mitochondrial pyrroline-5-carboxylate reductase 1 promotes invasiveness and impacts survival in breast cancers. *Carcinogenesis* **38**, 519–531 (2017).

55. Nusinow, D. P. *et al.* Quantitative Proteomics of the Cancer Cell Line Encyclopedia. *Cell* **180**, 387-402.e16 (2020).

56. Li, H., Barbour, J. A., Zhu, X. & Wong, J. W. H. Gene expression is a poor predictor of steady-state metabolite abundance in cancer cells. *FASEB J.* **36**, (2022).

57. Adelmann, C. H. *et al.* MFSD12 mediates the import of cysteine into melanosomes and lysosomes. *Nature* **588**, 699–704 (2020).

58. Reczek, C. R. *et al.* A CRISPR screen identifies a pathway required for paraquat-induced cell death. *Nat. Chem. Biol.* **13**, 1274–1279 (2017).

59. Park, M. H., Cooper, H. L. & Folk, J. E. Identification of hypusine, an unusual amino acid, in a protein from human lymphocytes and of spermidine as its biosynthetic precursor. *Proc. Natl. Acad. Sci.* **78**, 2869–2873 (1981).

60. Schuller, A. P., Wu, C. C. C., Dever, T. E., Buskirk, A. R. & Green, R. eIF5A Functions Globally in Translation Elongation and Termination. *Mol. Cell* **66**, 194-205.e5 (2017).

61. Suenkel, C., Cavalli, D., Massalini, S., Calegari, F. & Rajewsky, N. A Highly Conserved Circular RNA Is Required to Keep Neural Cells in a Progenitor State in the Mammalian Brain. *Cell Rep.* **30**, 2170-2179.e5 (2020).